Geochemical Perspectives Letters

© 2017 European Association of Geochemistry

Iodine proxy evidence for increased ocean oxygenation during the Bitter Springs Anomaly

W. Lu[1], S. Wörndle[2], G.P. Halverson[2], X. Zhou[1], A. Bekker[3], R.H. Rainbird[4], D.S. Hardisty[5], T.W. Lyons[3], Z. Lu[1*,6]

OPEN ACCESS

doi: 10.7185/geochemlet.1746

Abstract

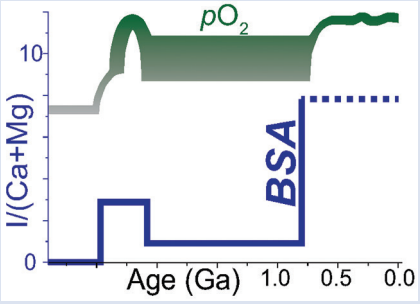

The Neoproterozoic Bitter Springs Anomaly (BSA; 810–800 Ma) is characterised by an 8 ‰ negative $\delta^{13}C$ excursion and is coeval with multiple indicators of increasing oxygenation of the ocean and atmosphere. Here, we use carbonate iodine contents to provide the first constraints on the evolution of local upper ocean redox conditions spanning the BSA. Iodine speciation in seawater is strongly redox sensitive, and carbonates precipitated proximal to O_2-depleted water record low I/(Ca + Mg). Data from the Akademikerbreen Group of Svalbard show a major rise of I/(Ca + Mg) during the recovery phase of the BSA. Other relatively high I/(Ca + Mg) values are also associated with rising $\delta^{13}C$ throughout the section. Combined with existing palaeoredox proxies (*e.g.*, Cr and S isotopes), our new iodine data most likely reflect an oxygenation event.

Received 22 June 2017 | Accepted 13 November 2017 | Published 18 December 2017

Introduction

The second largest rise in atmospheric oxygen in Earth's history might have occurred during the Neoproterozoic Era or the Palaeozoic (*e.g.*, Lyons *et al.*, 2014; Sperling *et al.*, 2015). The Neoproterozoic is distinguished by dramatic palaeoenvironmental and biological changes, manifested in a pair of global glaciations, extreme fluctuations in $\delta^{13}C$ values of seawater, and the emergence of macroscopic animals (Macdonald *et al.*, 2010). The *ca.* 810–800 Ma Bitter Springs Anomaly (BSA) is a long-lived negative excursion in seawater $\delta^{13}C$ (Halverson *et al.*, 2005). The BSA is broadly coeval with a proposed eukaryotic diversification event, as well as an inferred rise in atmospheric O_2 (Fig. 1) (Planavsky *et al.*, 2014; Cohen and Macdonald, 2015; Thomson *et al.*, 2015; Cole *et al.*, 2016; Turner and Bekker, 2016). Consequently, understanding the change in ocean redox conditions during the BSA may provide important insights into the intertwined changes in the biosphere, atmospheric oxygen, and carbon cycle during this critical chapter in Earth history.

Bulk carbonate I/(Ca + Mg) is a local redox proxy that records upper ocean conditions where limestones and dolostones were formed. The thermodynamically stable forms of iodine in seawater are iodate (IO_3^-) and iodide (I^-) (Wong, 1991). Iodate is quantitatively converted to I^- in low O_2 settings such as oxygen minimum zones (OMZs) (Rue *et al.*, 1997). Further, IO_3^- is the only chemical form of iodine that is incorporated into the structure of carbonate minerals (Lu *et al.*, 2010), substituting for CO_3^{2-} (Podder *et al.*, 2017). Modern OMZs are characterised by low I/Ca (~0.5–2.5 µmol/mol) compared to that of the well-oxygenated waters (~5 µmol/mol) (Lu *et al.*, 2016). During Precambrian oxidation events in the relatively low pO_2 world (Fig. 1), dolostones rarely have I/(Ca + Mg) values above 2 µmol/mol (Hardisty *et al.*, 2017).

Here we present new I/(Ca + Mg) data (Fig. 1) from well-preserved carbonates of multiple outcrop sections in Svalbard and from a drill core in the Amundsen Basin of northwestern Canada (Supplementary Information and Fig. S-1). A previous study through this interval (of the lower Svanbergfjellet Formation) demonstrated that the dolomitisation of these samples was early, and fabric retentive, and that no subsequent alteration has overprinted the geochemical signatures of these rocks (Halverson *et al.*, 2007).

1. Department of Earth Sciences, Syracuse University, Syracuse, NY 13244, USA
2. Department of Earth and Planetary Sciences, McGill University, 3450 University St., Montreal, QC H3A 0E8, Canada
3. Department of Earth Sciences, University of California, Riverside, Riverside, CA 92521, USA
4. Geological Survey of Canada, 601 Booth Street, Ottawa, ON K1A 0E8, Canada
5. Department of Geology and Geophysics, Woods Hole Oceanographic Institute, Woods Hole, MA, USA
6. State Key Laboratory of Marine Environmental Science, Xiamen University, Xiamen 361102, China
* Corresponding author (email: zunlilu@syr.edu)

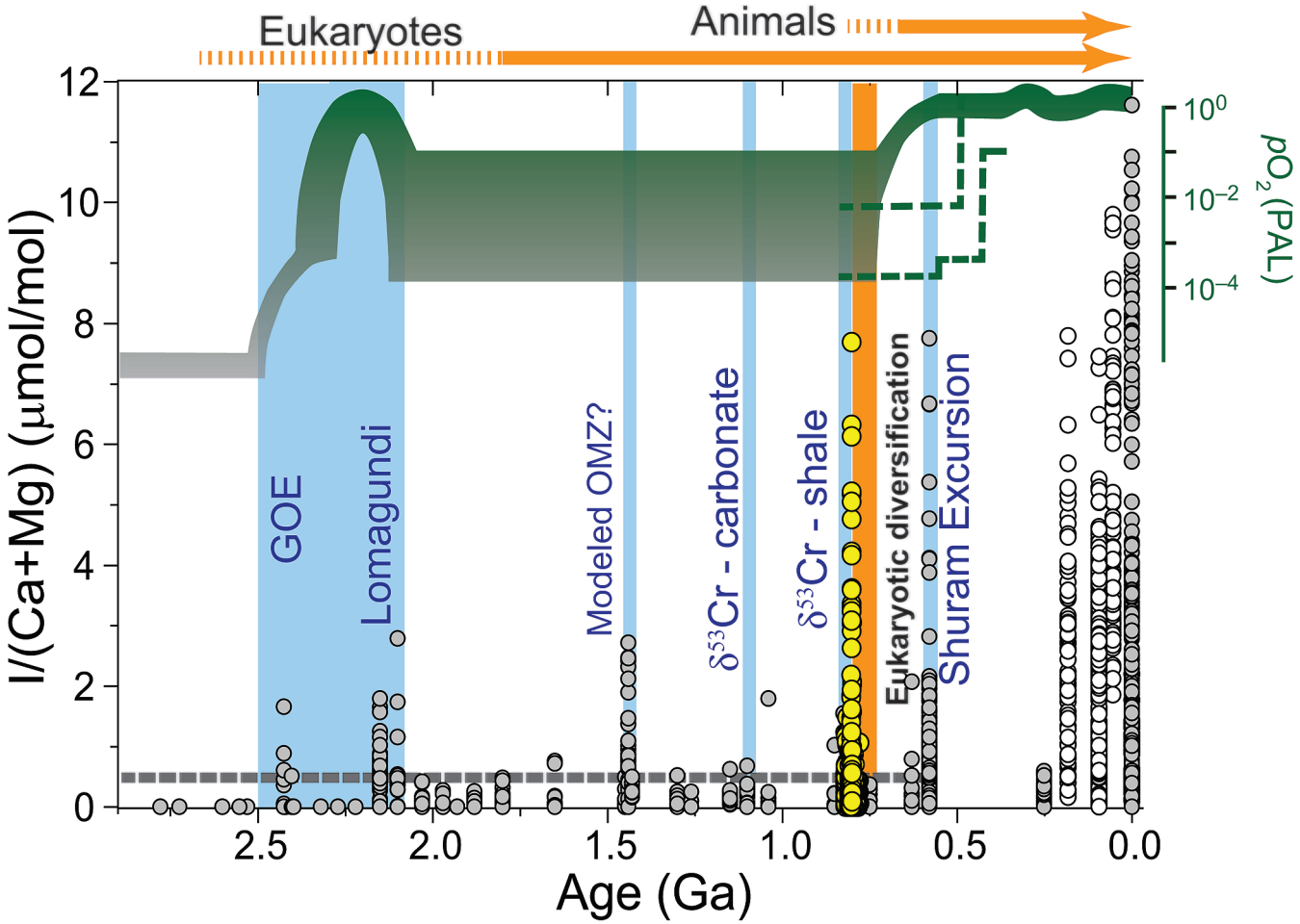

Figure 1 Secular trend of I/(Ca + Mg). White (I/Ca; limestone) and gray (I/(Ca + Mg); dolostone) dots are from Hardisty *et al.* (2017). Yellow dots are from this study. Blue bars mark intervals where there are data consistent with possible oxygenation events (Kendall *et al.*, 2009; Planavsky *et al.*, 2014; Gilleaudeau *et al.*, 2016) relative to the long term atmospheric pO_2 curve (green shades from Lyons *et al.*, 2014; green dash line from Sperling *et al.*, 2015) and major evolutionary events (orange) in biosphere. The grey dashed line at 0.5 µmol/mol is the Precambrian I/(Ca + Mg) baseline.

Methods

For the I/(Ca + Mg) analyses, ~4 mg of fine powder for each sample were weighed out and then rinsed with de-ionised water. Nitric acid (3 %) was added for dissolution. Fresh iodine calibration standards were prepared from potassium iodate powder. To stabilise iodine, 0.1 % tertiary amine solution was used after carbonate dissolution, followed immediately by measurements on a quadrupole ICP-MS (Bruker M90) at Syracuse University. The sensitivity of iodine was tuned to ~80 kcps for a 1 ppb standard. The precision for ^{127}I is normally better than 1 %. The long term accuracy is checked by frequently repeated analysis of the reference material JCp-1 (Lu *et al.*, 2010). The detection limit of I/Ca is on the order of 0.1 µmol/mol. Calcium and Mg concentrations were calibrated using a Merck multi-element standard and measured *via* ICP-MS.

Results

Excluding the samples from intervals with an oxygen rise suggested by other proxies, over 95 % of data (n = 250) from all previously published Proterozoic samples have I/(Ca + Mg) of < 0.5 µmol/mol, (Hardisty *et al.*, 2017). We therefore treat 0.5 µmol/mol as the baseline for I/(Ca + Mg) in Precambrian carbonates, marked by a dashed line in Figures 1 and 2. Values above this baseline are relatively high for the Proterozoic. The most prominent feature in our new dataset is a maximum in I/(Ca + Mg) reaching ~8 µmol/mol at the onset of the recovery phase of the BSA (Figs. 1 and 2). This peak greatly exceeds the maximum values found throughout the preceding Precambrian, including the Great Oxidation Event (GOE) at *ca.* 2.3–2.4 Ga (~2 µmol/mol; Hardisty *et al.*, 2014), but is comparable to the highest values recorded during the Ediacaran (*ca.* 580 Ma) Shuram Excursion (Hardisty *et al.*, 2017). In the Tonian Akademikerbreen Group, Svalbard, all but two samples with I/(Ca + Mg) values above 0.5 µmol/mol occur in intervals showing a prominent rise $\delta^{13}C$ (blue bars in Fig. 2a). In drill core samples from the Wynniatt Formation (Shaler Supergroup) in the Amundsen Basin (Thomson *et al.*, 2015), the iodine signal drops to zero during the BSA interval in organic matter-rich samples that have $\delta^{13}C$ values well below typical BSA values (Fig. 2c).

Discussion

Primary redox signal? Despite the potential for diagenetic resetting, the distinctively high I/(Ca + Mg) of the BSA in Svalbard compared to other Precambrian data is most likely a primary signal (Fig. 1) based on the following considerations:

(1) A plot of I/(Ca + Mg) against Mg/Ca (Fig. S-2, with a value of 1 for a pure dolomite end member) shows that the highest BSA I/(Ca + Mg) values from Svalbard are concentrated in partially to fully dolomitised samples. This is opposite of a

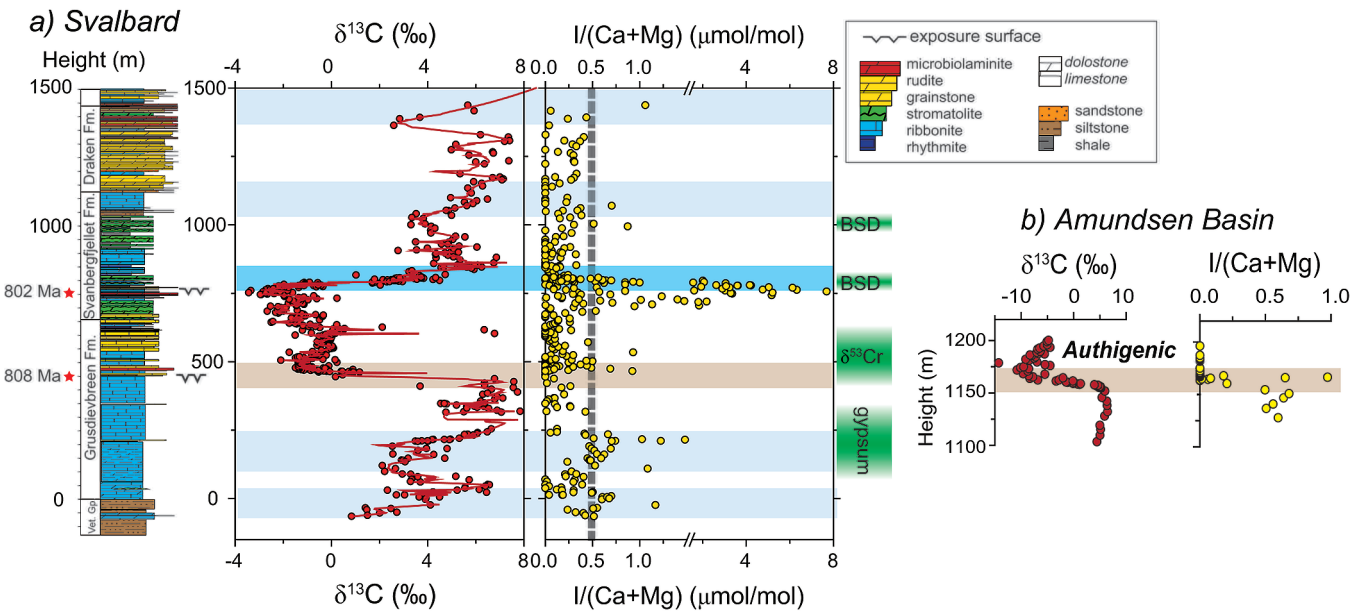

Figure 2 I/(Ca + Mg) data from **(a)** Svalbard and **(b)** Amundsen basin. Values above 0.5 µmol/mol (Fig. 1) are most commonly associated with the rise in $\delta^{13}C$ (blue bar). Darker blue bar highlights the recovery phase of BSA with a major increase in $\delta^{13}C$. The decrease in $\delta^{13}C$ that defines the base of the BSA is indicated with a brown bar, and data from Svalbard and the Amundsen Basin are lined up accordingly. Note the axis for I/(Ca + Mg) is broken at 1.50 to better illustrate stratigraphic trends below 2 µmol/mol. Green boxes show the timing of increases in O_2 levels as stratigraphically correlated to the Svalbard section. Gypsum evaporite deposits are from Turner and Bekker (2016). $\delta^{53}Cr$ signature is from Planavsky *et al.* (2014). BSD stands for bacterial sulphur disproportionation, as recorded in multiple sulphur isotope data (Kunzmann *et al.*, 2017).

trend observed in a comprehensive study of Neogene-Quaternary carbonates, which demonstrated that diagenesis, and most prominently dolomitisation, typically decreases the primary I/(Ca + Mg) signal (Hardisty *et al.*, 2017). Therefore, the I/(Ca + Mg) values that peak well above the baseline (Fig. 2) might have been higher initially prior to iodine loss during dolomitisation, *i.e.* the observed peak can be regarded as a minimum estimate of the changes in local seawater iodate level.

(2) In contrast to Svalbard, the BSA in the Amundsen Basin is associated with organic-rich carbonates marked by $\delta^{13}C_{carb}$ values (< -10 ‰) well below typical values for the BSA. These data suggest a large authigenic carbonate component (Thomson *et al.*, 2015). Authigenic carbonate in organic-rich sediments form in anoxic porewaters where I^- is the only iodine species and is excluded from the carbonate mineral lattice (Lu *et al.*, 2010). Hence, it is unsurprising that these Amundsen Basin samples yielded no detectable iodine (Fig. 2b). These Amundsen data confirm again (Hardisty *et al.*, 2017) that mixing authigenic carbonates into primary carbonates cannot cause a false positive in I/Ca values. The high I/(Ca + Mg) values in Svalbard samples, if associated with any authigenic components, should have had a primary signal higher than currently observed.

(3) Studies of recent carbonates from Bahamas (Clino) and the Pleistocene Key Largo limestone have found that carbonate recrystallisation during subaerial exposure and associated diagenesis in meteoric waters are most likely to reduce iodine in carbonates because iodine concentrations in fresh water are orders of magnitude lower than those in seawater (Hardisty *et al.*, 2017). Meteoric diagenesis during subaerial exposure also cannot explain the iodine spike observed for the BSA in Svalbard.

(4) The I/Ca spike is unlikely to be explained by shoaling of carbonate deposition (*e.g.*, near exposure surfaces) while maintaining the shallow oxycline conditions that typified most of parts of the Proterozoic. Firstly, all the Svalbard samples were preserved already at shallow depth (Halverson *et al.*, 2007). Secondly, the high I/(Ca + Mg) values are only associated with the upper subaerial exposure surface but not at the lower one (Fig. 2a). Finally, in the modern ocean, sea surface iodate concentrations are relatively low above a shallow OMZs (even at modern pO_2 level), resulting in I/Ca ratios below ~2.5 µmol/mol (Lu et al., 2016)—which stand in stark contrast to the observed very high BSA values of up to ~8 µmol/mol. Therefore, some fundamental redox reorganisation is likely required to account for the observed I/(Ca + Mg) spike during the BSA recovery.

Iodide oxidation during the BSA recovery. I/(Ca + Mg) ratios above 4 µmol/mol found in this study (Fig. 1) reach a range characteristic of Cenozoic and Mesozoic carbonate iodine records (Zhou *et al.*, 2015). We interpret these high I/(Ca + Mg) values during the BSA to reflect the oxidation of iodide in the upper ocean. Modern carbonate fossils show very low ratios of ~0.5 µmol/mol directly above strong and shallow OMZs, and >5 µmol/mol at well-oxygenated locations, indicating that I/Ca is a sensitive local to regional proxy for subsurface O_2-depletion and for the depth of oxycline in the water column (Lu *et al.*, 2016). Even though I/(Ca + Mg) is not a direct measure of atmospheric oxygen levels, the existing Precambrian I/(Ca + Mg) data show a response in the upper ocean to several possible oxygenation events identified based on other redox proxies (Fig. 1). This response is predicted because atmospheric pO_2 is one of the major controls on oxycline depth. I/(Ca + Mg) first rose to ~2 µmol/mol during the *ca.* 2.2–2.0 Ga Lomagundi Event following the GOE (Hardisty *et al.*, 2014). Relatively high values are also available from *ca.* 1.4 Ga carbonates in North China and the middle Ediacaran Shuram excursion (SE) (Hardisty *et al.*, 2017). Although carbon cycle dynamics and the primary controls on oxygenation were likely different during these three events, the increase in I/(Ca + Mg) that is common to all of them cannot be explained by diagenesis and likely reflects elevated oxygen levels. In this context, our I/(Ca + Mg) values up to ~8 µmol/mol during the BSA recovery are evidence for a remarkable increase in iodate

concentrations in the surface waters of a carbonate platform. The BSA I/(Ca + Mg) peak is most likely due to deepening of the oxycline and concomitant oxidation of iodide.

The I/(Ca + Mg) data suggest that the oxycline began to deepen slightly before the initial rise of $\delta^{13}C$ marking the onset of recovery from the BSA (darker blue bar in Fig. 2a). Similarly, there is evidence for shifting marine redox immediately prior to the positive $\delta^{13}C$ excursion due to global carbon burial defining the onset of Mesozoic Oceanic Anoxic Event 2 (Zhou *et al.*, 2015; Ostrander *et al.*, 2017; Owens *et al.*, 2017). Regardless of such an offset in timing, the I/(Ca + Mg) spike is tied stratigraphically most closely to the 8–10 ‰ increase in $\delta^{13}C$—rather than the 8 ‰ decrease in $\delta^{13}C$ that marks the initial phase of the BSA. More generally, carbonates with I/(Ca + Mg) above the Precambrian baseline (0.5 µmol/mol) are mostly restricted to intervals with rising $\delta^{13}C$ values in the Akademikerbren Group (Fig. 2a, light blue bars). These observations imply that iodide oxidation events occurred repeatedly during the middle Neoproterozoic and were coupled to both the carbon cycle and upper ocean redox.

Broader landscape of Neoproterozoic oxygenation. There is independent evidence that our observed elevated I/(Ca + Mg) values record a significant transition to more oxidising conditions (Fig. 2a). Thick gypsum deposits occur just below the BSA interval in early Neoproterozoic basins on at least three cratons, following a prolonged interval of sparse gypsum evaporite deposition (Turner and Bekker, 2016). This sharp increase in gypsum deposition is interpreted to reflect a build-up of marine sulphate levels due to an increase in oxidative weathering of the continents or a decrease in pyrite burial prior to the BSA—both of which are consistent with higher atmospheric oxygen levels. Chromium isotope ($\delta^{53}Cr$) data from ironstones and shales suggest very low atmospheric O_2 throughout the mid-Proterozoic up to *ca*. 0.8 Ga (Planavsky *et al.*, 2014; Cole *et al.*, 2016). Based on carbon isotope chemostratigraphy, the increase in $\delta^{53}Cr$ was initiated prior to the onset of the BSA and hence precedes the I/(Ca + Mg) peak in the Akademikerbreen Group in Svalbard. Furthermore, multiple sulphur isotope data delineate signatures of bacterial sulphur disproportionation in the middle Neoproterozoic, suggesting at least local oxidative sulphur cycling prior to more widespread oxidative cycling beginning in the early Ediacaran Period (Kunzmann *et al.*, 2017). Each of these redox indicators reflects different processes, controls, and challenges, yet they consistently imply oxygenation in the atmosphere-ocean system at approximately 800 Ma.

Following the BSA, I/(Ca + Mg) values in the Akademikerbreen Group returned to levels mostly below the Proterozoic baseline. Similar trends are recorded for the other Precambrian events marked by elevated I/(Ca + Mg) (Hardisty *et al.*, 2017), suggesting a pattern of dynamic behaviour, with long term deepening of the oxycline occurring much later in Earth history. Such a pattern of episodic (transient) Neoproterozoic oxygenation is also observed in other proxy records such as S, Mo, and Fe (Dahl *et al.*, 2010; Sperling *et al.*, 2015; Kunzmann *et al.*, 2017). This relationship implies a fundamental instability in oxygen levels that may have extended into, and through, the Ediacaran and perhaps into the Palaeozoic (Sperling *et al.*, 2015; Sahoo *et al.*, 2016). The details of this behaviour and its possible implications for the life emerging remain targets for future research.

Acknowledgements

ZL, WL, XZ acknowledge NSF EAR-1349252 and OCE-1232620. GH and RR acknowledge support from NSERC Discovery grants. AB acknowledges NSERC Discovery and Accelerator Grants as well as the support from the Society of Independent Thinkers. Funds from the NSF and the NASA Astrobiology Institute supported the contributions of DH and TL.

Editor: Liane G. Benning

Additional Information

Supplementary Information accompanies this letter at www.geochemicalperspectivesletters.org/article1746

This work is distributed under the Creative Commons Attribution 4.0 License, which permits unrestricted use, distribution, and reproduction in any medium, provided the original author and source are credited. Additional information is available at http://www.geochemicalperspectivesletters.org/copyright-and-permissions.

Cite this letter as: Lu, W., Wörndle, S., Halverson, G.P., Zhou, X., Bekker, A., Rainbird, R.H., Hardisty, D.S., Lyons, T.W., Lu, Z. (2017) Iodine proxy evidence for increased ocean oxygenation during the Bitter Springs Anomaly. *Geochem. Persp. Let.* 5, 53–57.

References

Cohen, P.A., Macdonald, F.A. (2015) The Proterozoic Record of Eukaryotes. *Paleobiology* 41, 610–632.

Cole, D.B., Reinhard, C.T., Wang, X., Gueguen, B., Halverson, G.P., Gibson, T., Hodgskiss, M.S.W., McKenzie, N.R., Lyons, T.W., Planavsky, N.J. (2016) A shale-hosted Cr isotope record of low atmospheric oxygen during the Proterozoic. *Geology* 44, 555–558.

Dahl, T.W., Hammarlund, E.U., Anbar, A.D., Bond, D.P.G., Gill, B.C., Gordon, G.W., Knoll, A.H., Nielsen, A.T., Schovsbo, N.H., Canfield, D.E. (2010) Devonian rise in atmospheric oxygen correlated to the radiations of terrestrial plants and large predatory fish. *Proceedings of the National Academy of Sciences of the United States of America* 107, 17911–17915.

Gilleaudeau, G.J., Frei, R., Kaufman, A.J., Kah, L.C., Azmy, K., Bartley, J.K., Chernyavskiy, P., Knoll, A.H. (2016) Oxygenation of the mid-Proterozoic atmosphere: clues from chromium isotopes in carbonates. *Geochemical Perspectives Letters* 2, 178–187.

Halverson, G.P., Hoffman, P.F., Schrag, D.P., Maloof, A.C., Rice, A.H.N. (2005) Toward a Neoproterozoic composite carbon-isotope record. *Geological Society of America Bulletin* 117, 1181–1207.

Halverson, G.P., Maloof, A.C., Schrag, D.P., Dudas, F.O., Hurtgen, M.T. (2007) Stratigraphy and geochemistry of a ca 800 Ma negative carbon isotope interval in northeastern Svalbard. *Chemical Geology* 237, 5–27.

Hardisty, D.S., Lu, Z., Planavsky, N., Bekker, A., Philippot, P., Zhou, X., Lyons, T.W. (2014) An iodine record of Paleoproterozoic surface ocean oxygenation. *Geology* 42, 619–622.

Hardisty, D.S., Lu, Z., Bekker, A., Diamond, C.W., Gill, B.C., Jiang, G., Kah, L.C., Knoll, A.H., Loyd, S.J., Osburn, M.R., Planavsky, N.J., Wang, C., Zhou, X., Lyons, T.W. (2017) Perspectives on Proterozoic surface ocean redox from iodine contents in ancient and recent carbonate. *Earth and Planetary Science Letters* 463, 159–170.

Kendall, B., Creaser, R.A., Gordon, G.W., Anbar, A.D. (2009) Re–Os and Mo isotope systematics of black shales from the Middle Proterozoic Velkerri and Wollogorang Formations, McArthur Basin, northern Australia. *Geochimica et Cosmochimica Acta* 73, 2534–2558.

Kunzmann, M., Bui, T.H., Crockford, P.W., Halverson, G.P., Scott, C., Lyons, T.W., Wing, B.A. (2017) Bacterial sulfur disproportionation constrains timing of Neoproterozoic oxygenation. *Geology* 45, 207–210.

Lu, Z., Jenkyns, H.C., Rickaby, R.E.M. (2010) Iodine to calcium ratios in marine carbonate as a paleo-redox proxy during oceanic anoxic events. *Geology* 38, 1107–1110.

Lu, Z., Hoogakker, B.A.A., C.D., H., Zhou, X., Thomas, E., Gutchess, K., Lu, W., Jones, L., Rickaby, R.E.M. (2016) Oxygen depletion recorded in upper waters of the glacial Southern Ocean. *Nature Communications* 7, 11146.

Lyons, T.W., Reinhard, C.T., Planavsky, N.J. (2014) The rise of oxygen in Earth's early ocean and atmosphere. *Nature* 506, 307–315.

Macdonald, F.A., Schmitz, M.D., Crowley, J.L., Roots, C.F., Jones, D.S., Maloof, A.C., Strauss, J.V., Cohen, P.A., Johnston, D.T., Schrag, D.P. (2010) Calibrating the Cryogenian. *Science* 327, 1241–1243.

Ostrander, C.M., Owens, J.D., Nielsen, S.G. (2017) Constraining the rate of oceanic deoxygenation leading up to a Cretaceous Oceanic Anoxic Event (OAE-2: ~94 Ma). *Science Advances* 3, e1701020.

Owens, J.D., Lyons, T.W., Hardisty, D.S., Lowery, C.M., Lu, Z., Lee, B., Jenkyns, H.C. (2017) Patterns of local and global redox variability during the Cenomanian–Turonian Boundary Event (Oceanic Anoxic Event 2) recorded in carbonates and shales from central Italy. *Sedimentology* 64, 168–185.

Planavsky, N.J., Reinhard, C.T., Wang, X.L., Thomson, D., McGoldrick, P., Rainbird, R.H., Johnson, T., Fischer, W.W., Lyons, T.W. (2014) Low Mid-Proterozoic atmospheric oxygen levels and the delayed rise of animals. *Science* 346, 635–638.

Podder, J., Lin, J., Sun, W., Botis, S.M., Tse, J., Chen, N., Hu, Y., Li, D., Seaman, J., Pan, Y. (2017) Iodate in calcite and vaterite: Insights from synchrotron X-ray absorption spectroscopy and first-principles calculations. *Geochimica et Cosmochimica Acta* 198, 218–228.

Rue, E.L., Smith, G.J., Cutter, G.A., Bruland, K.W. (1997) The response of trace element redox couples to suboxic conditions in the water column. *Deep-Sea Research Part I-Oceanographic Research Papers* 44, 113–134.

Sahoo, S.K., Planavsky, N.J., Jiang, G., Kendall, B., Owens, J.D., Wang, X., Shi, X., Anbar, A.D., Lyons, T.W. (2016) Oceanic oxygenation events in the anoxic Ediacaran ocean. *Geobiology* 14, 457–468.

Sperling, E.A., Wolock, C.J., Morgan, A.S., Gill, B.C., Kunzmann, M., Halverson, G.P., Macdonald, F.A., Knoll, A.H., Johnston, D.T. (2015) Statistical analysis of iron geochemical data suggests limited late Proterozoic oxygenation. *Nature* 523, 451–454.

Thomson, D., Rainbird, R.H., Planavsky, N., Lyons, T.W., Bekker, A. (2015) Chemostratigraphy of the Shaler Supergroup, Victoria Island, NW Canada: A record of ocean composition prior to the Cryogenian glaciations. *Precambrian Research* 263, 232–245.

Turner, E.C., Bekker, A. (2016) Thick sulfate evaporite accumulations marking a mid-Neoproterozoic oxygenation event (Ten Stone Formation, Northwest Territories, Canada). *Geological Society of America Bulletin* 128, 203–222.

Wong, G.T.F. (1991) The marine geochemistry of iodine. *Reviews in Aquatic Sciences* 4, 45–73.

Zhou, X., Jenkyns, H.C., Owens, J.D., Junium, C.K., Zheng, X., Sageman, B., Hardisty, D.S., Lyons, T.W., Ridgwell, A., Lu, Z. (2015) Upper ocean oxygenation dynamics from I/Ca ratios during the Cenomanian-Turonian OAE 2. *Paleoceanography* 30, 510–526.

Geochemical Perspectives Letters

© 2017 European Association of Geochemistry

Iodine proxy evidence for increased ocean oxygenation during the Bitter Springs Anomaly

W. Lu[1], S. Wörndle[2], G.P. Halverson[2], X. Zhou[1], A. Bekker[3], R.H. Rainbird[4], D.S. Hardisty[5], T.W. Lyons[3], Z. Lu[1*,6]

Supplementary Information

The Supplementary Information includes:

- The BSA and Sample Materials
- Dolomitisation
- Table S-1
- Figures S-1 and S-2
- Supplementary Information References

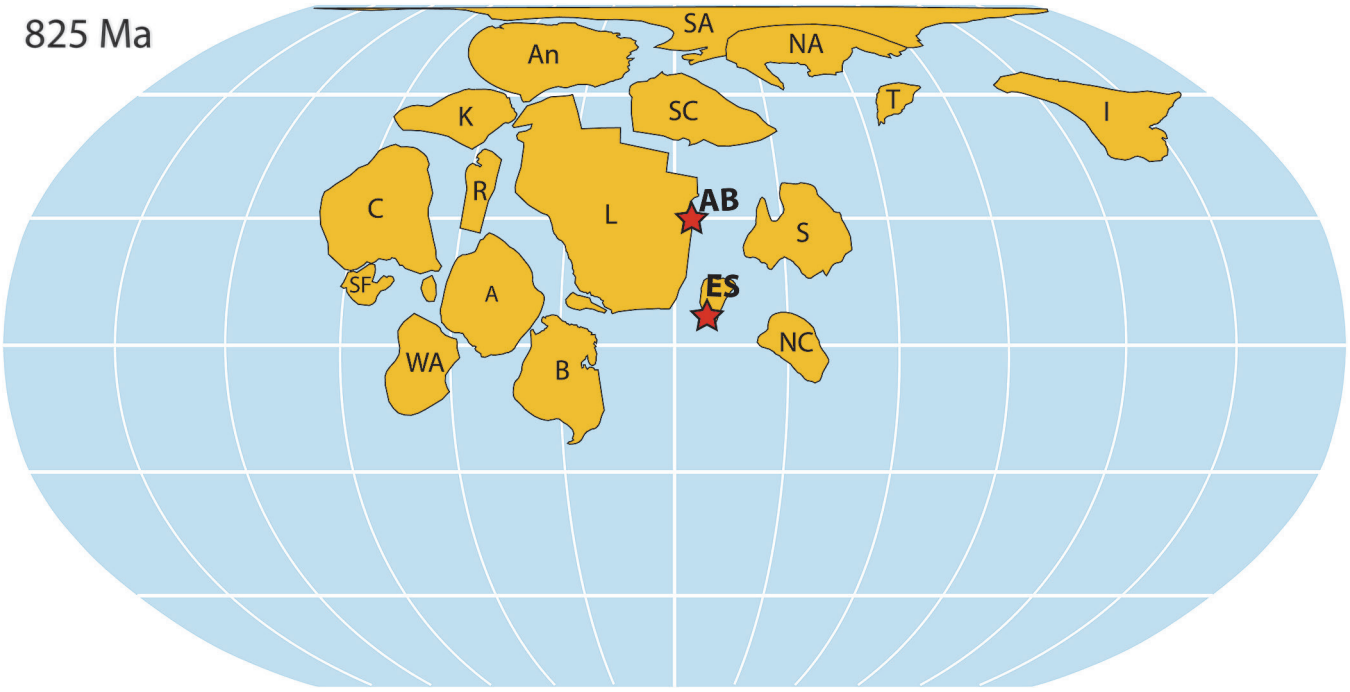

Figure S-1 Palaeogeographic reconstruction for 825 Ma (modified from Li *et al.*, 2013). Stars mark sampled locations (*ES* = East Svalbard; *AB* = Amundsen Basin). Craton names: A = Amazon; An = Antarctica; B = Baltica; C = Congo; I = India; K = Kalahari; NA = northern Australia; R = Rio Plata; S = Siberia; SA = southern Australia; SC = South China; T = Tarim; WA = West Africa.

1. Department of Earth Sciences, Syracuse University, Syracuse, NY 13244, USA
2. Department of Earth and Planetary Sciences, McGill University, 3450 University St., Montreal, QC H3A 0E8, Canada
3. Department of Earth Sciences, University of California, Riverside, Riverside, CA 92521, USA
4. Geological Survey of Canada, 601 Booth Street, Ottawa, ON K1A 0E8, Canada
5. Department of Geology and Geophysics, Woods Hole Oceanographic Institute, Woods Hole, MA, USA
6. State Key Laboratory of Marine Environmental Science, Xiamen University, Xiamen 361102, China
* Corresponding author (email: zunlilu@syr.edu)

The BSA and Sample Materials

The BSA anomaly has been documented in basins on multiple cratons, and radiometric age constraints from northwestern Canada (Macdonald *et al.*, 2010) and Ethiopia (Swanson-Hysell *et al.*, 2015), along with Sr isotope data, indicate that it records a global and long-lived perturbation to seawater that began *ca.* 810 Ma. In Svalbard, where it is documented in the greatest detail (Halverson *et al.*, 2007), the BSA is defined at the base by a negative 8 ‰ shift in $\delta^{13}C$ that spans a minor subaerial unconformity in the middle Grusdievbreen Formation. Low $\delta^{13}C$ values (-4 to 0 ‰) persist for ~300 m of section deposited over 5–10 Myr (Swanson-Hysell *et al.*, 2015), and a shift back to high $\delta^{13}C$ (>5 ‰) occurs in a transgressive systems tract above a second subaerial unconformity within the lower Svanbergfjellet Formation.

$\delta^{13}C$ data presented here are from four formations in the Akademikerbreen Group, spanning the BSA: the Grusdievbreen, Svanbergfjellet, Draken, and Backlundtoppen formations. We plot the data as a single composite section, constructed by correlating individual partial sections, using well defined formation and member boundaries that can be easily identified across the outcrop belt (Knoll and Swett, 1990; Halverson *et al.*, 2005). Most of the carbon isotope data shown in Figure 2 were previously published (Halverson *et al.*, 2005, 2007); however, some new data from previously studied stratigraphic sections are included. The new data were acquired on sample powders in the McGill Stable Isotope Laboratory on a Nu Instruments Perspective dual inlet mass spectrometer, coupled to a NuCarb automated carbonate preparation device. The reproducibility of standards was typically better than 0.1 ‰.

Dolomitisation

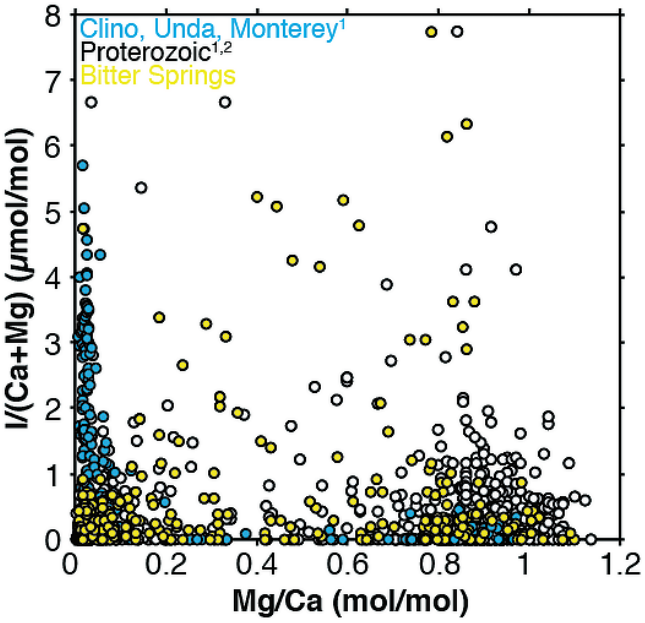

Figure S-2 I/(Ca + Mg) *vs.* Mg/Ca. Blue data points for multiple Neogene diagenetic scenarios (Hardisty *et al.*, 2017). White circles for Proterozoic carbonates (Hardisty *et al.*, 2017). Yellow points are from this study.

Data Table

Table S-1 is available for download as an Excel file at http://www.geochemicalperspectivesletters.org/article1746.

Table S-1 I/(Mg + Ca) and δ13C data from **(a)** Svalbard and **(b)** the Amundsen Basin.

Supplementary Information References

Halverson, G.P., Hoffman, P.F., Schrag, D.P., Maloof, A.C., Rice, A.H.N. (2005) Toward a Neoproterozoic composite carbon-isotope record. *Geological Society of America Bulletin* 117, 1181–1207.

Halverson, G.P., Maloof, A.C., Schrag, D.P., Dudas, F.O., Hurtgen, M. (2007) Stratigraphy and geochemistry of a ca 800 Ma negative carbon isotope interval in northeastern Svalbard. *Chemical Geology* 237, 5–27.

Hardisty, D.S., Lu, Z., Bekker, A., Diamond, C.W., Gill, B.C., Jiang, G., Kah, L.C., Knoll, A.H., Loyd, S.J., Osburn, M.R., Planavsky, N.J., Wang, C., Zhou, X., Lyons, T.W. (2017) Perspectives on Proterozoic surface ocean redox from iodine contents in ancient and recent carbonate. *Earth and Planetary Science Letters* 463, 159–170.

Knoll, A.H., Swett, K. (1990) Carbonate deposition during the late Proterozoic era - an example from Spitsbergen. *American Journal of Science* 290A, 104–132.

Li, Z.X., Evans, D.A.D., Halverson, G.P. (2013) Neoproterozoic glaciations in a revised global palaeogeography from the breakup of Rodinia to the assembly of Gondwanaland. *Sedimentary Geology* 294, 219–232.

Macdonald, F.A., Schmitz, M.D., Crowley, J.L., Roots, C.F., Jones, D.S., Maloof, A.C., Strauss, J.V., Cohen, P.A., Johnston, D.T., Schrag, D.P. (2010) Calibrating the Cryogenian. *Science* 327, 1241–1243.

Swanson-Hysell, N.L., Maloof, A.C., Condon, D.J., Jenkin, G.R.T., Alene, M., Tremblay, M.M., Tesema, T., Rooney, A.D., Haileab, B. (2015) Stratigraphy and geochronology of the Tambien Group, Ethiopia: Evidence for globally synchronous carbon isotope change in the Neoproterozoic. *Geology* 43, 323–326.